Chapter 3

Electron collisions with the D-molecules and H_2SO_4

The present chapter covers the results of various inelastic cross-sections (Q_{inel}, Q_{ion} and ΣQ_{exc}) for the deuterated molecules (D-molecules) and sulfuric acid (H_2SO_4) for the impact energies from molecular ionisation energy to 5000 eV. Various correlation study on the Q_{ion} and polarisability of the D-molecules has also been attempted. Isotope effect for the deuterated and respected protonated molecules has also been studied here.

3.1 D-molecules

By researching the density of water in 1931, H.C. Urey made the discovery of deuterium (D). Deuterium (D), an isotope of hydrogen, has drawn a lot of interest in the scientific community due to its notable isotope effect without any radioactive characteristics. Deuterium research has been conducted for about a century. Throughout history, the demand for war, drove the promotion and development of nuclear weapons, which in turn spurred the rapid development of deuterium research. The worldwide movement towards disarmament, replaced the cold war's central theme with peace and ushered in a new age of peaceful economic prosperity. Under these conditions, deuterium application research switched to a significant extent to the disciplines of engineering and natural sciences. Deuterium can be utilised in military applications to create deuterium-fluoride (DF) laser weapons, neutron bombs, and hydrogen bombs. Apart from military applications, deuterium is now also widely employed in nuclear medicine, controlled nuclear fusion reactions, deuterated lubricants,

deuterated optical fibres, nuclear energy, lightbulbs, lasers, novel drug synthesis, and much more [1].

Like other molecules, the electron impact collisions with deuterated molecules lead to many elastics as well as inelastic processes. Among all of these processes, the most effective and fundamental channel for probing the structure and dynamics of the target molecules is ionisation and undoubtedly in a variety of applications such as, astrophysics, plasma physics, planetary sciences, radiation sciences etc. [2–5], the total ionisation cross-sections for electron collisions with molecules have taken the centre stage.

The electron interactions with these deuterated compounds lead to numerous elastic and inelastic processes, much like in case of other molecules. However, ionization among all of these processes, is the most efficient and fundamental tool for examining the dynamics and structure of the target systems and various applications of its ionisation cross-sections, including plasma physics, astrophysics, radiation sciences, planetary sciences etc., thrust it into the limelight [2–5].

3.1.1 Literature survey

Deuterated molecules HD, D_2, D_2O, ND_x (x=1-3), SiD_x (x=1-3), and CD_x (x=2-4) have been selected for the present study because, in addition to their wide range of applications in diverse disciplines, these molecules have received less attention (Table 3.1).

Table 3.1 Literature survey relevant to present work (IE - ionisation energy)

Sr	Target	Quantity	Energy (eV)	Method of investigation	Reference
1	HD	-	-	-	-
2	D_2	Total Q_{ion}	IE-1000	Experimental method	Rapp and Englander-Golden [6]
			IE-500	Experimental method	Cowling and Fletcher [7]
			600-20000	Experimental (Condenser technique)	Schram *et.al.* [8]
			IE-170	Experimental (crossed molecule-	Märk and

3	D_2O	Parent Q_{ion}		electron beam apparatus)	Egger [9]
			IE-120	Experimental (quadrupole mass-spectrometric technique)	Snegursky and Zavilopulo [10]
		Parent Q_{ion}, Partial Q_{ion}	IE-200	Experimental (Fast-neutral-beam-technique)	Tarnovsky *et.al.* [11]
		Partial and Total Q_{ion}	IE-1000	Experimental method	Straub *et.al.* [12]
		Total Q_{ion}	15-150	Experimental method	N. Lj. Djuric *et al.* [13]
4	ND_3	Parent Q_{ion}	IE-200	Experimental (Fast-neutral-beam-technique)	Tarnovsky *et.al.* [14]
		Total Q_{ion}	IE-1000	Theoretical (using DM formalism, BEB method and calculation of Saksena)	Rejoub *et.al.* [15]
		Partial Q_{ion}		Experimental method	
5	ND, ND_2	Partial Q_{ion}	IE-200	Experimental (Fast-neutral-beam-technique)	Tarnovsky *et.al.* [14]
6	SiD, SiD_2, SiD_3	Partial Q_{ion}	IE-200	Experimental (Fast-neutral-beam-technique)	Tarnovsky *et.al.* [16]
7	CD_4	Total Q_{ion}	600-20000	Experimental (Condenser technique)	Schram *et.al.* [17]
		Partial Q_{ion}	IE-200	Experimental (Fast-neutral-beam-technique)	Tarnovsky *et.al.* [18]
8	CD_2, CD_3	Partial Q_{ion}	IE-200	Experimental (Fast-neutral-beam-technique)	Tarnovsky *et.al.* [18]
				Experimental (Crossed-beams apparatus)	Baiocchi *et.al.* [19]

3.1.2 Theoretical Methodology

In the present work, SCOP and CSP-ic approaches have been employed to calculate the probabilities of inelastic processes, including ionisations and excitations, occurring during the interaction of electrons and D-molecules. As all potentials (V_s, V_{ex}, V_p, and V_{ab}) are

constructed using the molecular charge density $\rho(r)$, it is crucial to describe it (see chapter 2). We introduced parameterized charge densities of constituent atoms through Hartree Fock wave functions [20] and used single-centre (SC) approximation for HD, D_2, D_2O, and ND_x (x=1-3) and modified additivity rule (MAR) for SiD_x (x=1-3) and CD_x (x=2-4) in order to construct the total $\rho(r)$ of the molecules under study, which is then fed to construct the optical complex potential (V_c). The atomic charge densities are superimposed on the molecular centre of mass in the cases of SC and MAR. The necessary input parameters for molecules are provided in Table 3.2.

Table 3.2 Molecular properties of present targets

Target	IE (eV)	Bond length (A°)	Target	IE (eV)	Bond length (A°)
HD	15.44 [21a]	0.7410 [21a]	SiD	07.89 [16]	-
D_2	15.47 [21a]	0.7420 [21a]	SiD_2	08.92 [16]	-
D_2O	12.64 [21a]	0.9687 [22]	SiD_3	08.14 [16]	-
ND	13.49 [14]	1.0367 [23a]	CD_2	10.40 [19]	-
ND_2	11.45 [21a]	1.0240 [21a]	CD_3	09.83 [18]	-
ND_3	10.08 [21a]	1.0026 [21a]	CD_4	12.51 [18]	-

3.1.3 Results and Discussion

For families of deuterated compounds including HD, D_2, D_2O, ND_x (x=1-3), SiD_x (x=1-3), and CD_x (x=2-4), we present the cross-section results of three major inelastic events during electron collisions with D-molecules through Q_{inel}, Q_{ion} and Q_{exc}. We also discuss the isotope effect and the correlation between Q_{ion} and dipole polarisability (α), which results in a prediction of for ND and SiD_x (x=1-3) that is not previously reported in the literature [23b].

A. Inelastic processes

HD and D_2 (singly and doubly deuterated hydrogen molecules)

The singly and doubly deuterated hydrogen molecules, HD and D_2, respectively, are famous for their crucial contribution in both planetary atmospheres and star formation. In the

interstellar medium, HD is the third-most abundant molecule (ISM). Moreover, it has been discovered that HD can be found in the environment of Jupiter, Neptune, Uranus, and Saturn [4].

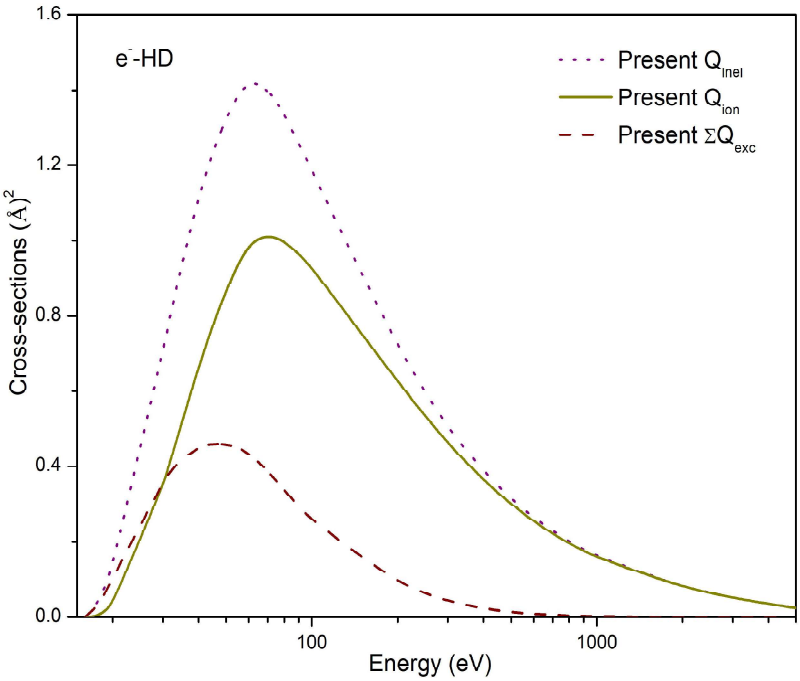

Figure 3.1 e^- - HD collision cross-sections

Dots: Present Q_{inel}; Solid: Present total Q_{ion}; Dash: Present $\sum Q_{exc}$

Additionally, key components in the tokamak edge plasmas are HD and D_2 [24–26]. Hence, a thoroughly verified database of the cross-sections for electron interaction with HD and D_2 molecules is necessary to clarify the numerous processes that take place in the tokamak edge plasma.

For the molecules HD and D_2, figures 3.1 and 3.2 display the plots of the cross-section data vs incident electron energy (E_i), which ranges from IE to 5000 eV. The curves at the top and bottom of each picture show the HD and D_2 molecules' Q_{inel} and Q_{exc}, respectively. To the best of our knowledge, this is the first effort to report HD molecule cross-sections data. Figure 3.1 displays the current total Q_{ion} data for the electron collision with the HD molecule. The calculated electron cross-sections for the D_2 molecule is likewise missing. The Q_{ion} for the D_2 molecule were reported experimentally by Rapp and Englander-Golden [6], Cowling and Fletcher [7], and Schram et al. [8]. Our Q_{ion} data and those of Rapp and Englander-Golden [6] and Cowling and Fletcher [7] are in good agreement at the peak region. The

current total Q_{ion} shows very good matching with Schram *et.al.* [8] experimental findings in higher energy regimes. Yoon *et.al.* [27] have also reviewed the HD and D_2 cross-section data.

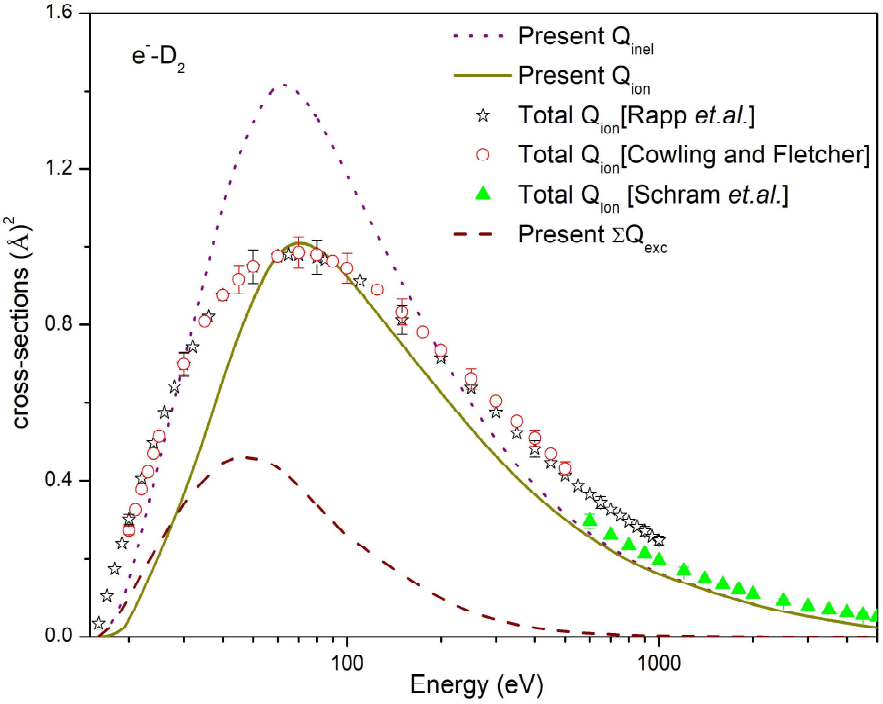

Figure 3.2 e^- - D_2 collision cross-sections

Dot: Present Q_{inel}; Solid: Present total Q_{ion}; Stars: total Q_{ion} [6]*; Open circles: total Q_{ion}* [7]*; Filled triangle: total Q_{ion}* [8]*; Dash: Present $\sum Q_{exc}$.*

D_2O (heavy water molecule)

D_2O, a "heavy water" molecule, is an intriguing "sister" to the regular H_2O molecule [10]. The wide technological applicability of the D_2O molecule as a coolant in nuclear power plants, as well as its usage in NMR spectroscopy and chemical research utilising synchrotron radiation, where D atoms are employed in place of H atoms in some compounds, and so on, has led us to see it as a critical and fascinating substance. Furthermore, D_2O has been found in celestial environments [28]. Thus, research into electron collisions with heavy water is necessary to comprehend processes that occur in the terrestrial environment. In addition to being a unique functional material, our motivation for performing these computations came from the absence of cross-section data.

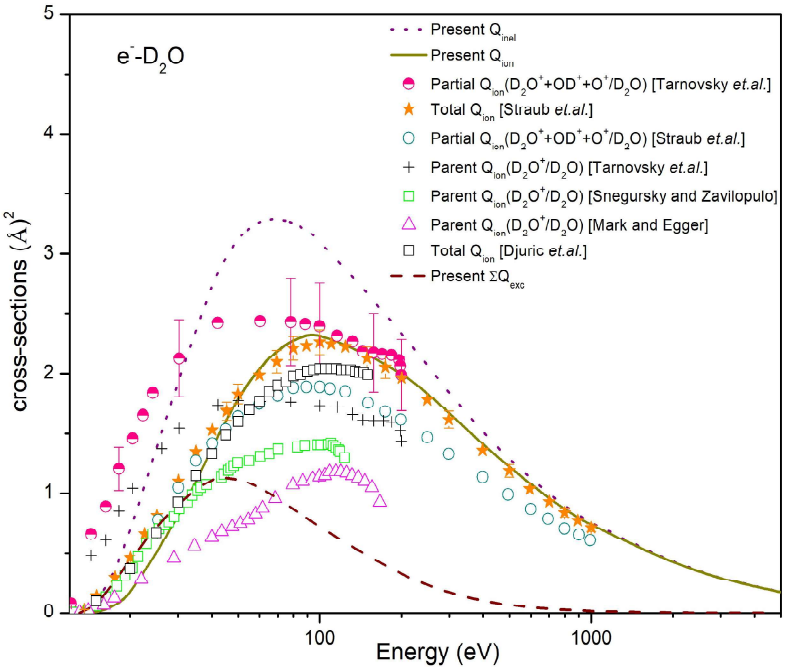

Figure 3.3 e^- - D_2O collision cross-sections

Dots: Present Q_{inel}; Solid: Present total Q_{ion}; Half-filled circles: Partial Q_{ion} ($D_2O^+ + OD^+ + O^+/D_2O$) [11]*; Filled stars: Total Q_{ion}* [12]*; Open circles: Partial Q_{ion} ($D_2O^+ + OD^+ + O^+/D_2O$)* [12]*; Plus: Parent Q_{ion} (D_2O^+/D_2O)* [11]*; Open squares: Parent Q_{ion} (D_2O^+/D_2O)* [10]*; Open triangle: Parent Q_{ion} (D_2O^+/D_2O)* [9]*; Open square: Total Q_{ion}* [29]*; Dash: Present $\sum Q_{exc}$*

Figure 3.3 depicts the present cross-sections results for D_2O along with the available experimental data. There are no theoretical cross-sections data available for this molecule. Figure 3.3 shows an excellent agreement between the present total Q_{ion} and the experimental total Q_{ion} of Straub *et.al.* [12] within the reported uncertainty of 4.5%. The experimental results for total Q_{ion} measured by N. J. Djuric *et.al.* [13] using a parallel plate ionisation chamber are lower than the present one at the peak region. However, a good match can be seen in the lower energy regime. Straub *et.al.* [12] and Tarnovsky *et.al.* [11] measured the partial Q_{ion} ($D_2O^+ + OD^+ + O^+/D_2O$). Present Q_{ion} matches favourably at the peak region, with Tarnovsky *et.al.* [11] partial Q_{ion}, measured within 15% uncertainty, whereas partial Q_{ion} data of [12] underestimates the present Q_{ion}, since the present total Q_{ion} covers all ionisation channels. The absolute parent ionisation cross-sections (D_2O^+/D_2O) were measured by Märk and Egger [9], Tarnovsky *et.al.* [11], and Snegursky and Zavilopulo [10]. As expected, all of these absolute parent Q_{ion} (D_2O^+/D_2O) [9–11] are lower than the present Q_{ion}. Figure 3.3

also depicts the total Q_{inel} and Q_{exc} using the present methodology, for which no comparison is available.

ND_x (x=1-3) family

Various ammonia isotopes, including ND_3, have been discovered in dense cloud cores (Barnad 1 [30] and NGC 1333 [31]) in the interstellar medium (ISM). ND has also been detected in the ISM near the young solar mass protostar IRAS16293 [32] and in the prestellar core 16293E [33]. Ammonia is also employed in the production of nitride films as a supply of nitrogen atoms. However, due to advancements in deuterium-based semiconductor devices, ND_3 is also being employed in place of NH_3 [34].

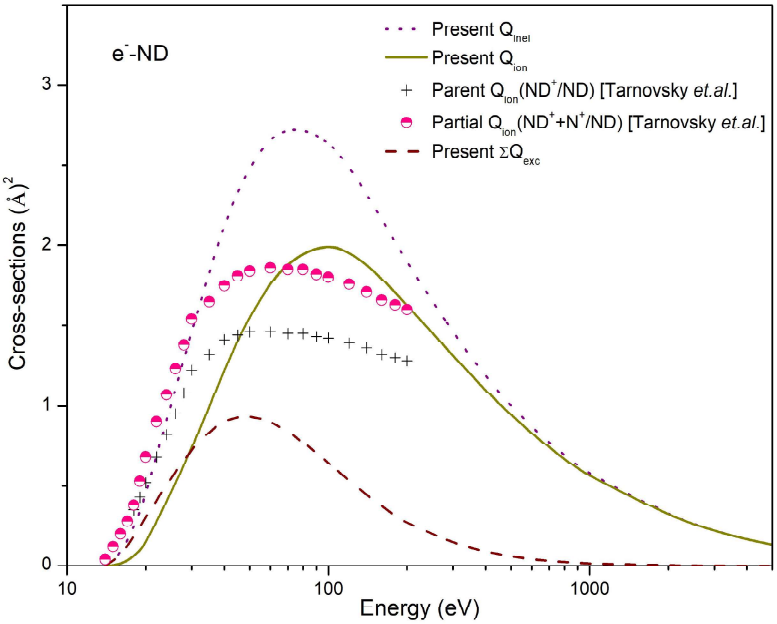

Figure 3.4 e^- - ND collision cross-sections

Dots: Present Q_{inel}; Solid: Present total Q_{ion}; Plus: Parent Q_{ion} (ND^+/ND) [14]*; Half-filled circles: Partial Q_{ion} (ND^++N^+/ND)* [14]*; Dash: Present* $\sum Q_{exc}$.

Figures 3.4, 3.5, and 3.6 show the present Q_{inel}, total Q_{ion}, and Q_{exc} data with the available comparisons for the ND_x (x=1-3) molecules. There is also a dearth of theoretical and experimental cross-section data for ND and ND_2 radicals in this area. Only Tarnovsky *et.al.* [14] reported the absolute parent (ND^+/ND and ND_2^+/ND_2) and partial (ND^+ + N^+/ND and ND_2^+ + ND^+/ND_2) ionisation cross-sections for the ND and ND_2 radicals depicted in figures

3.4 and 3.5. By adding the absolute Q_{ion} data for the ND^+ and N^+ fragment ions from the ND radical and the ND_x^+ (x=1,2) fragment ions from the ND_2 radical [14], the partial Q_{ion} depicted in figures 3.4 and 3.5 are obtained by us. As expected, all of these partial Q_{ion} and parent Q_{ion} data exhibit lower values than the current total Q_{ion} data.

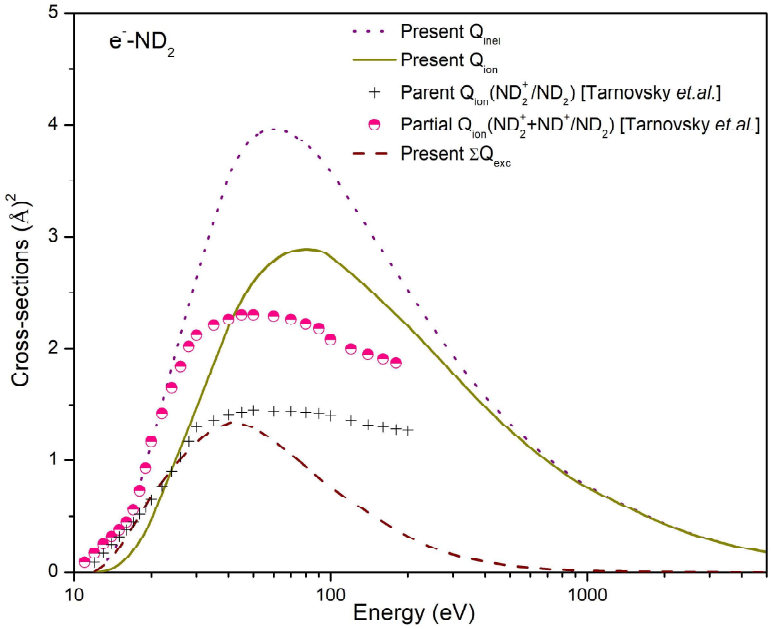

Figure 3.5 e^- - ND_2 collision cross-sections

Dots: Present Q_{inel}; Solid: Present total Q_{ion}; Plus: Parent Q_{ion} (ND_2^+/ND_2) [14]*; Half-filled circles: Partial Q_{ion} ($ND_2^+ + ND^+/ND_2$)* [14]*; Dash: Present $\sum Q_{exc}$.*

The data of cross-sections for the ND_3 molecule are presented in Figure 3.6. The absolute partial and parent ionisation cross-section measurements for the generation of various fragment ions from the parent ND_3 molecule were measured by Rejoub *et.al.* [15]. For the sake of brevity, they are not depicted in figure 3.6. They reported the calculated and experimental data for total Q_{ion} as well [15]. The calculations of Saksena *et.al.*, the Deutsch-Märk formalism, and the Binary-encounter-Bethe model, were used by Rejoub *et.al.* [15] to estimate the total Q_{ion}. In the energy range of the current investigation, our Q_{ion} results exhibit excellent agreement with the experimental and theoretical data of Rejoub *et.al.* [15]. The measured absolute parent (ND_3^+/ND_3) and partial Q_{ion} ($ND_3^+ + ND_2^+/ND_3$) data of Tarnovsky *et.al.* [14] underestimate the present total Q_{ion} data as expected. These partial Q_{ion} data were

produced by adding the two absolute single Q_{ion} data [14] for the generation of ND_x^+ (x=2-3) fragment ions from ND_3 parent molecule.

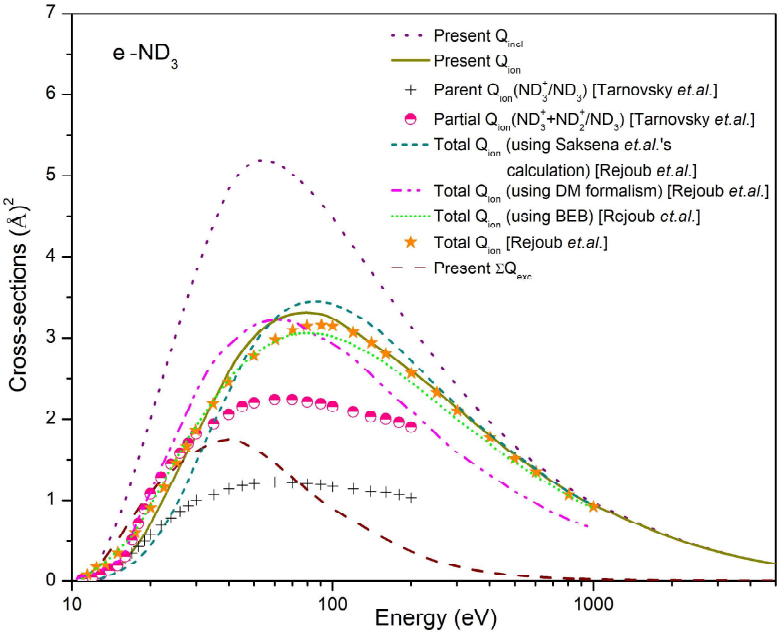

Figure 3.6 e^- - ND_3 collision cross-sections

Dots: Present Q_{inel}; Solid: Present total Q_{ion}; Plus: Parent Q_{ion} (ND_3^+/ND_3) [14]*; Half-filled circles: Partial Q_{ion} ($ND_3^+ + ND_2^+/ND_3$)* [14]*; Short Dash line: Total Q_{ion} (Saksena et.al.'s calculation)* [15]*; Dash-Dot-Dot line: Total Q_{ion} (DM formalism)* [15]*; Short Dot line: Total Q_{ion} (BEB method)* [15]*; Filled stars: Total Q_{ion}* [15]*; Dash: Present $\sum Q_{exc}$.*

SiD_x (x=1-3) family

The major weakness in silicon hydrogenated films is the effects associated with the de-passivation of hot carrier effects (e.g., electrons). Deuterium conditioning of semiconductors has been demonstrated to be successful in reducing such effects. When deuterium is used in place of hydrogen for the passivation of the devices, it is found that the degradation of the threshold voltage and transconductance is dramatically reduced, increasing the practical lifetime of the devices by a factor of 10–50 and opening the door to operating the semiconductor devices at higher voltages [35–37]. To gain a thorough understanding of the deposition process of deuterated amorphous silicon films, which are often created by

Chemical Vapour Deposition (CVD) techniques, a systematic study of tiny clusters of Si and D (for example, SiDx (x=1-3)) is necessary.

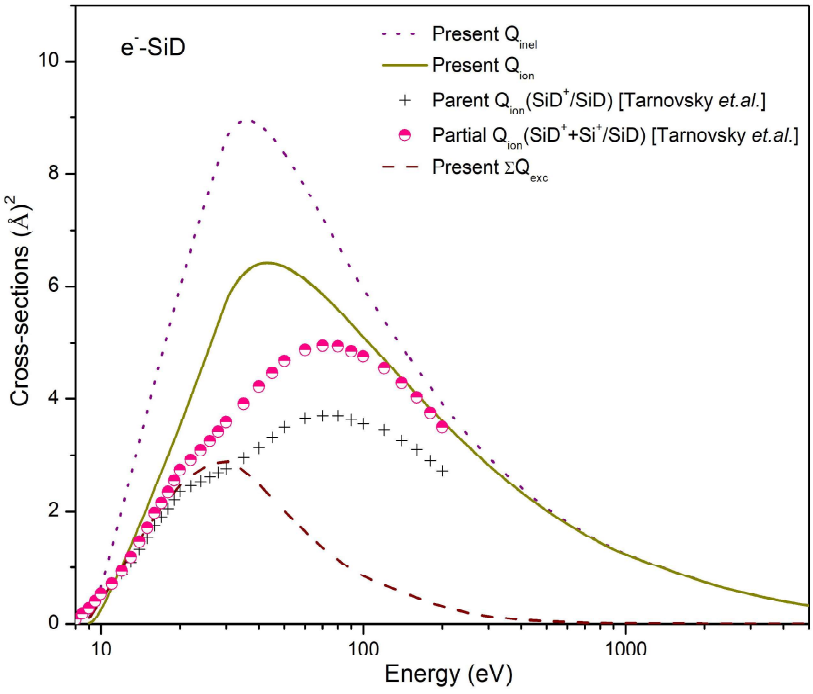

Figure 3.7 e^- - SiD collision cross-sectios

Dots: Present Q_{inel}; Solid: Present total Q_{ion}; Plus: Parent Q_{ion} (SiD^+/SiD) [16]*; Half-filled circles: Partial Q_{ion} ($SiD^+ + Si^+/SiD$)* [16]*; Dash: Present $\sum Q_{exc}$*

For SiDx (x=1-3) molecules, the present computed results are shown in figures 3.7, 3.8, and 3.9 respectively. This is the first attempt to present the cross-section data for molecules of SiD_x (x=1-3). The only measurement of the absolute parent (SiD^+/SiD, SiD_2^+/SiD_2, and SiD_3^+/SiD_3) and partial ions ($SiD^+ + Si^+/SiD_2$, $SiD_3^+ + SiD_2^+/SiD_3$) for the generation of SiD_x^+ (x=1-3) and Si^+ fragment ions from SiD_x (x=1-3) molecules was reported by Tarnovsky *et.al.* [16]. The present Q_{ion} data is also compared to the partial Q_{ion} data [16] for SiD (summation of absolute single Q_{ion} for the formation of $SiD^+ + Si^+$ fragments from SiD), SiD_2 (summation of absolute single Q_{ion} for the formation of $SiD_2^+ + SiD^+$ from SiD_2), and SiD_3 (summation of absolute single Q_{ion} for the formation of $SiD_3^+ + SiD_2^+$). The partial Q_{ion} and absolute parent Q_{ion} of Tarnovsky *et.al.* [16] for SiD_x (x=1-3) molecules are overestimated by the current Q_{ion} data because they account for all potential ionisation processes.

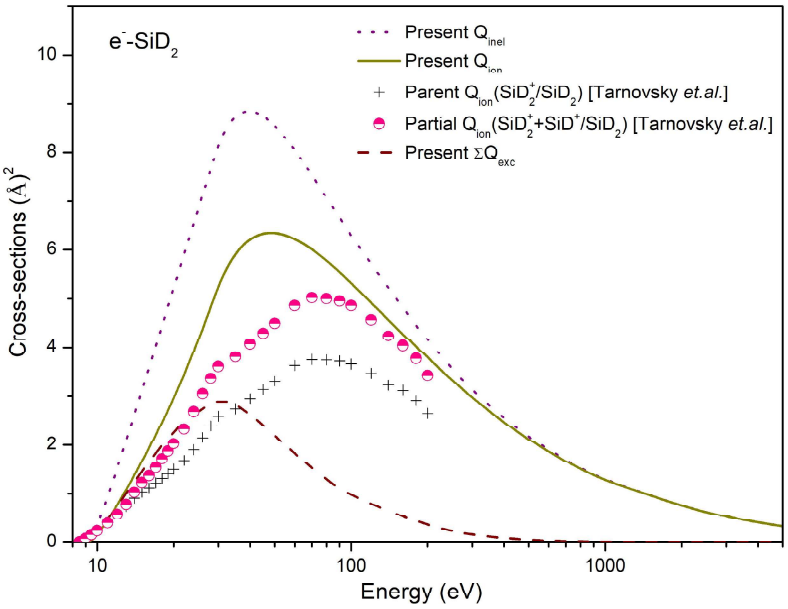

Figure 3.8 e^- - SiD_2 collision cross-sections

Dots: Present Q_{inel}; Solid: Present total Q_{ion}; Plus: Parent Q_{ion} (SiD_2^+/SiD_2) [16]; Half-filled circles: Partial Q_{ion} ($SiD_2^+ + SiD^+/SiD_2$) [16]; Dash: Present $\sum Q_{exc}$.

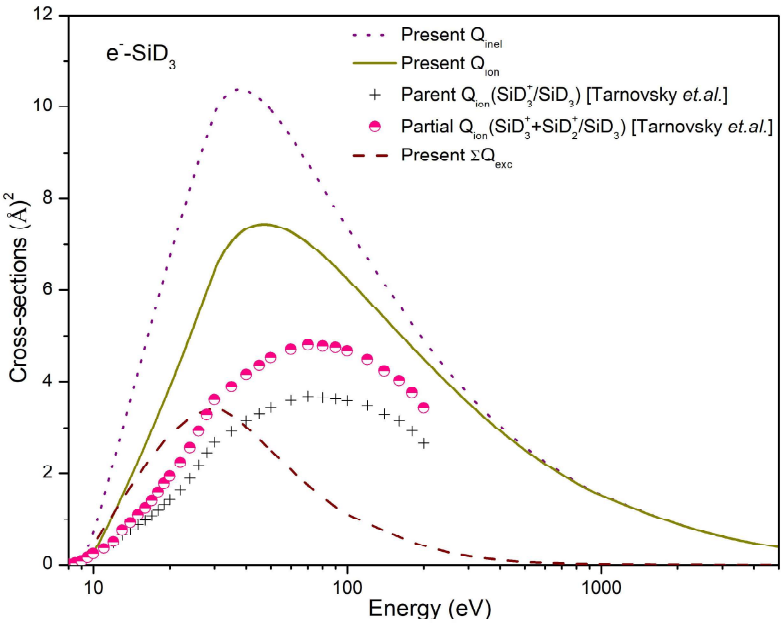

Figure 3.9 e^- - SiD_3 collision cross-sections

Dots: Present Q_{inel}; Solid: Present Q_{ion}; Plus: Parent Q_{ion} (SiD_3^+/SiD_3) [16]*; Half-filled circles: Partial Q_{ion} ($SiD_3^+ + SiD_2^+/SiD_3$)* [16]*; Dash: Present $\sum Q_{exc}$*

CD_x (x=2-4) family

Deuterium-containing amorphous carbon materials can be used to create optical waveguide devices with low loss light transmission at specific wavelengths that are commonly used in optical telecommunications. Plasma Enhanced Chemical Vapour Deposition (PECVD) techniques, which use volatile deutero-carbon precursors, e.g., CD_4 etc., deposit amorphous deuterated carbon material [38]. Also, a comprehensive database of cross-sections for all interaction events influencing the fragmentation of hydrocarbons is required for a thorough modelling of the transport of hydrocarbons in divertor plasmas in tokamaks. The family of deutero-methane CD_x (x=1-4) molecular ions plays a significant role among all existing molecular ions [39,40].

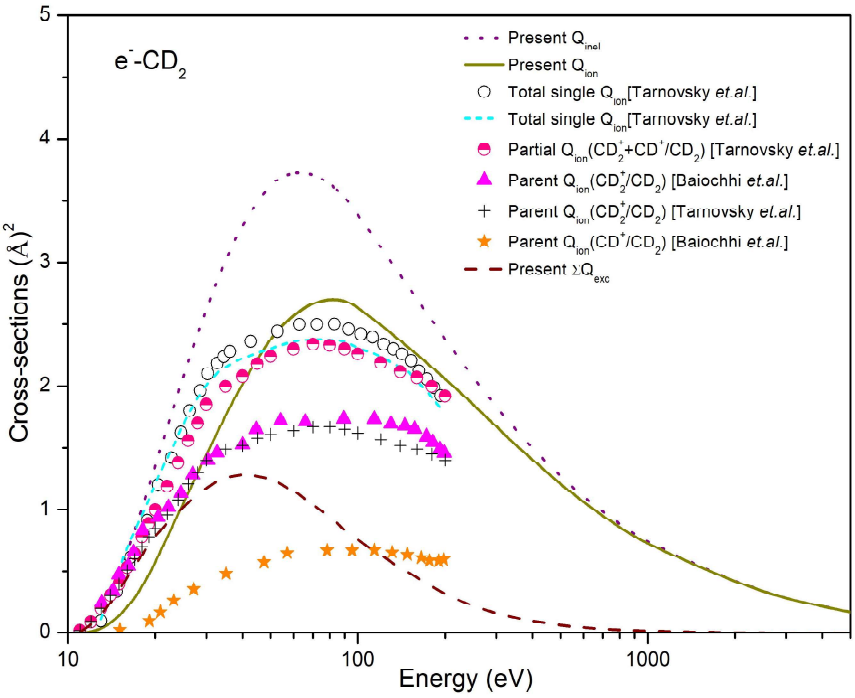

Figure 3.10 e^- - CD_2 collision cross-sections

Dots: Present Q_{inel}; Solid: Present Q_{ion}; Open circle: Total single Q_{ion} [18]*; Short Dash line: Total single Q_{ion}* [18]*; Half-filled circles: Partial Q_{ion} (CD_2^++CD^+/CD_2)* [18]*; Filled triangles: Parent Q_{ion} (CD_2^+/CD_2)* [19]*; Plus: Parent Q_{ion} (CD_2^+/CD_2)* [18]*; Filled stars: Parent Q_{ion} (CD^+/CD_2)* [19]*; Dash: Present $\sum Q_{exc}$*

The cross-section data for the CD_x (x=2-4) molecules are plotted in Figures 3.10, 3.11, and 3.12 with an energy range of IE to 5000 eV, respectively. For these compounds, there is a lack of existing data. According to our literature review, no total Q_{ion} results for CD_2 and CD_3 radicals have been reported (Table 3.1). Experimentally, Tarnovsky *et.al.* [18] and Baiochhi *et.al.* [19] reported the absolute partial Q_{ion} ($CD_2^+ + CD^+/CD_2$ and $CD_3^+ + CD_2^+/CD_3$) for the generation of CD_x^+ (x=1-2) from CD_2 radical and CD_x^+ (x=2,3) from CD_3 radical. Along with the parent Q_{ion} and partial Q_{ion} results of Tarnovsky *et.al.* [18] and Baiochhi *et.al.* [19] for the CD_2 and CD_3 radicals, the present computed total Q_{ion} is displayed in figures 3.10 and 3.11, respectively.

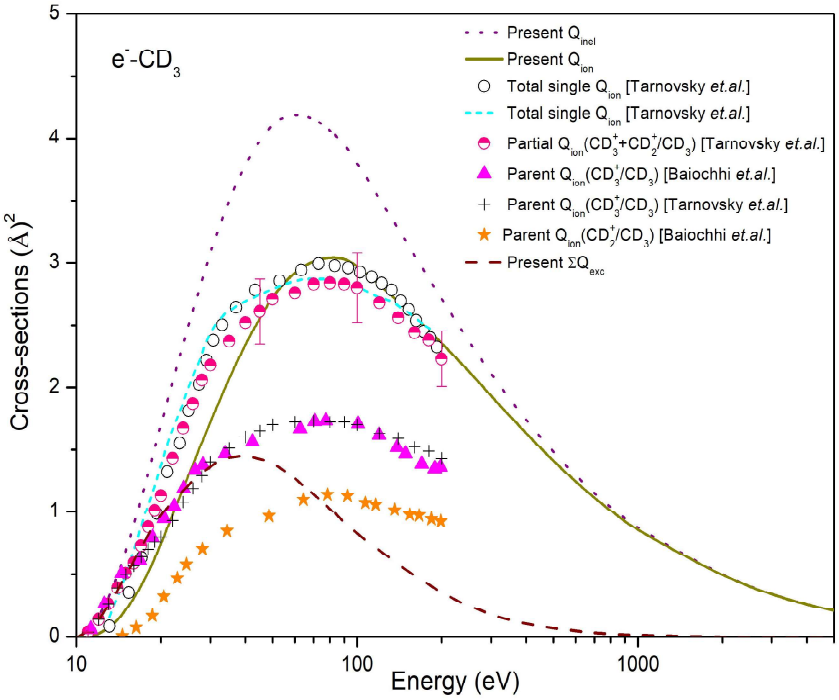

Figure 3.11 e^- - CD_3 collision cross-sections

Dots: Present Q_{inel}; Solid: Present total Q_{ion}; Open circle: Total single Q_{ion} [18]*; Short Dash line: Total single Q_{ion}* [18]*; Half-filled circles: Partial Q_{ion} (CD_3^+ + CD_2^+/CD_3)* [18]*; Filled triangles: Parent Q_{ion} (CD_3^+/CD_3)* [19]*; Plus: Parent Q_{ion} (CD_3^+/CD_3)* [18]*; Filled stars: Parent Q_{ion} (CD_2^+/CD_3)* [19]*; Dash: Present $\sum Q_{exc}$.*

In addition, Tarnovsky *et.al.* [18] provided the total single Q_{ion} for CD_2 and CD_3 radicals both theoretically and practically (measured partial Q_{ion} were added by them). These total single Q_{ion} values are close to the current Q_{ion}. According to Tarnovsky *et.al.* [14], the cross

section of generation of parent or fragment ions with multiple charges is smaller than that of parent or fragment ions with a single charge. As a result, the total single Q_{ion}, which is the cross section of all singly charged ions, is comparable to the current total Q_{ion}. Comparable partial Q_{ion} data for CD_2 (CD_2^+ + CD^+/CD_2) and CD_3 (CD_3^+ + CD_2^+/CD_3) are also included. All of the data for absolute parent and partial Q_{ion} had lower values than the current total Q_{ion}.

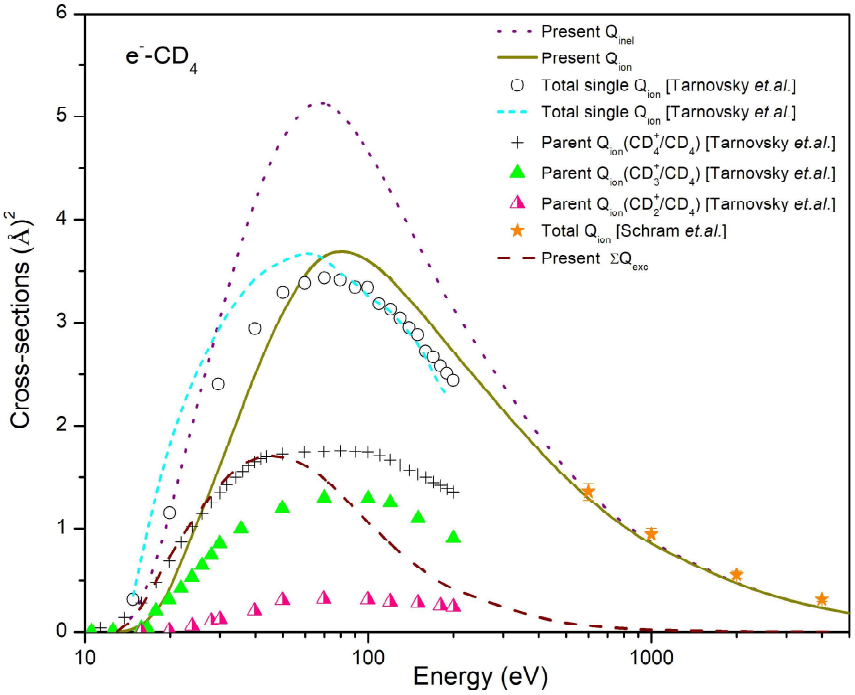

Figure 3.12 e^- - CD_4 collision cross-sections

Dots: Present Q_{inel}; Solid: Present total Q_{ion}; Open circle: Total single Q_{ion} [18]*; Short Dash line: Total single Q_{ion}* [18]*; Plus: Parent Q_{ion} (CD_4^+/CD_4)* [18]*; Filled triangles: Parent Q_{ion} (CD_3^+/CD_4)* [19]*; Half-filled triangle: Parent Q_{ion} (CD_2^+/CD_4)* [18]*; Filled stars: Total Q_{ion}* [17]*; Dash: Present $\sum Q_{exc}$*

Figure 3.12 depicts a plot of CD_4 molecule cross-section data. Only Schram *et.al.* [17] performed the experimental measurement for absolute total Q_{ion} of CD_4 in the energy range 600-20000 eV. Their data is in excellent accord with present Q_{ion} results. Tarnovsky *et.al.* [18] experimentally evaluated the absolute parent Q_{ion} for the generation of CD_x^+ (x=2-4) fragment ions from CD_4. In figure 3.12, we plotted our total Q_{ion} data against three kinds of parent Q_{ion} [18]. All of these parent Q_{ion} [18] are, as expected, of lower values than the present total Q_{ion}. They also reported total single Q_{ion} for CD_4 [18], both theoretically and

experimentally, and both of which compare favourably with the present total Q_{ion}, particularly in the peak region, as anticipated by Tarnovsky *et.al.* [14].

B. Isotope effect

The isotope effect for the electron induced ionisations of the molecules, the scattering cross-section of which (Q_{ion}) is an applied quantity, is what we are attempting to see in this subsection. We computed Q_{ion} for H_2, H_2O, NH_3, SiH_3, and CH_4 and compared them to the Q_{ion} for their deuterated counterparts in order to explore this impact. The ratio of Q_{ion} for deuterated to protonated molecules is seen in table 3.3.

Table 3.3 Ratio of Q_{ion} for deuterated and corresponding protonated molecules

E_i (eV)	D_2/H_2	D_2O/H_2O	ND_3/NH_3	SiD_3/SiH_3	CD_4/CH_4
9	-	-	-	0.9231	-
11	-	-	1.0000	0.9932	-
13	-	0/0	1.0000	0.9968	0/0
16	0/0	1.0000	0.9943	0.9982	1.1194
18	1.0000	0.9987	0.9951	0.9983	1.0697
20	0.9394	1.0000	0.9945	0.9984	1.0537
60	0.9917	1.0027	0.9952	0.9995	1.0143
100	0.9942	1.0012	0.9967	0.9998	1.0104
500	0.9966	0.9992	0.9981	0.9996	1.0089
1000	0.9937	0.9986	0.9979	0.9993	1.0072
5000	1.0000	1.0000	1.0000	1.0000	1.0055

The total ionisation cross-sections are sensitive to the molecular charge cloud size via the Z electron number of the target and the ionisation threshold of the molecule. We notice that Q_{ion} is not dependent on isotopes. This is to be expected given that the calculation includes the electronic charge density and the first ionisation energy of the target molecules, and the first ionisation energies of these deuterated molecules and their protonated counterparts are nearly identical. Figures 3.13 and 3.14 compare the Q_{ion} values for D_2O and H_2O and ND_3 and NH_3, respectively, to provide a clear understanding.

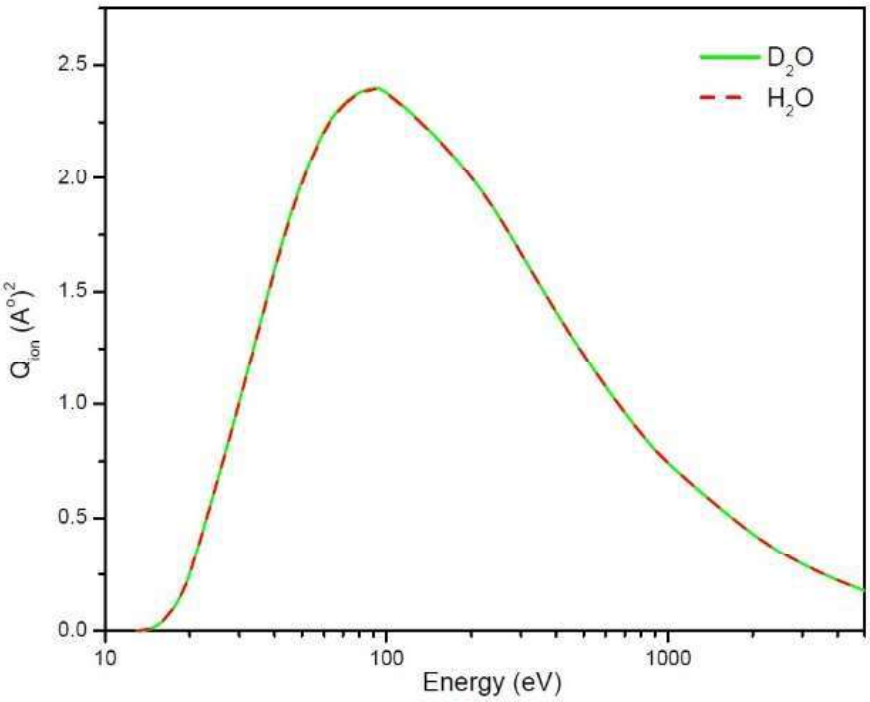

Figure 3.13 Comparison of Q_{ion} between D_2O and H_2O

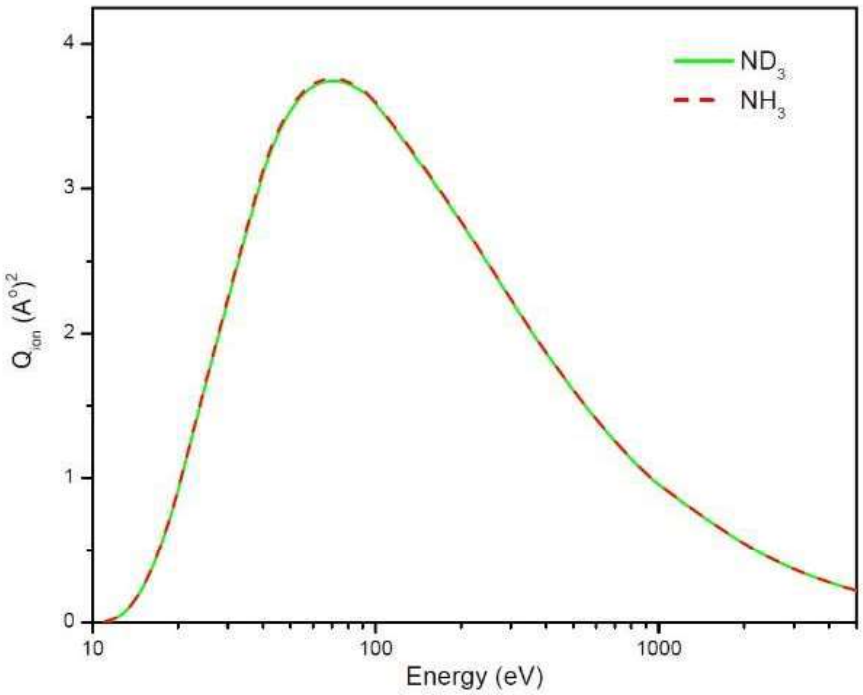

Figure 3.14 Comparison of Q_{ion} between ND_3 and NH_3

C. Prediction of polarisability

We investigated the relationship between maximum Q_{ion} and polarizability (α) for the present studied targets. Figure 3.15 depicts the linear relationship established by Harland and Vallance [41] between Q_{ion} (peak) and polarisability (α) using the following fitting equation,

$$Q_{ion}(peak) = 1.5510\ \alpha - 0.1178 \qquad (R^2 = 0.9968)$$

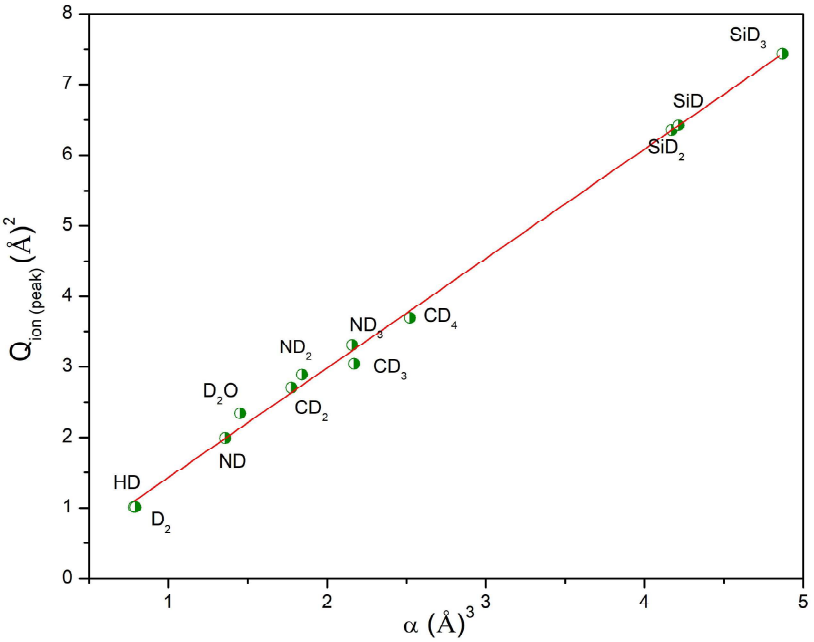

Figure 3.15 Correlation between Q_{ion} (peak) and polarisability (α)

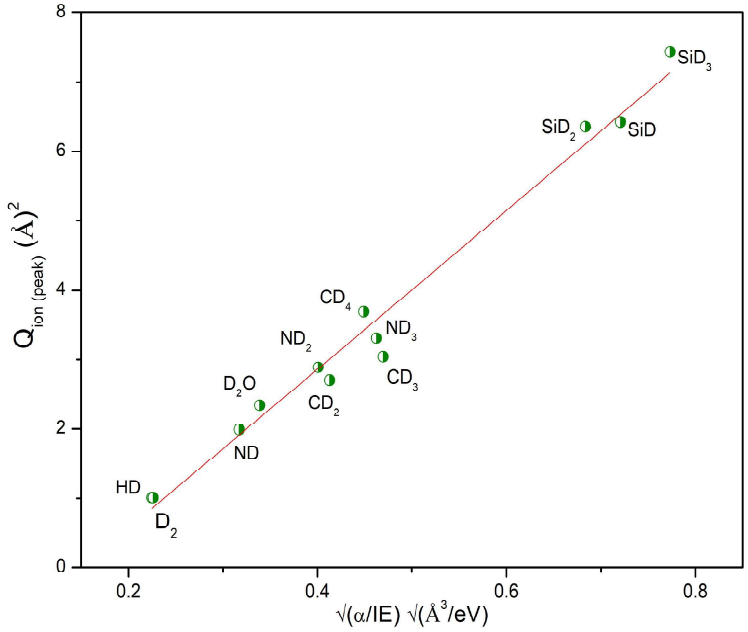

Figure 3.16 Correlation between Q_{ion} (peak) and $\sqrt{\alpha/IE}$

Figure 3.16 displays the plot of Q_{ion} (peak) value against $\sqrt{\alpha/IE}$, and the least squares fit exhibits a strong association with

$$Q_{ion}(peak) = 11.4475\sqrt{\alpha/IE} - 1.7195 \qquad (R^2 = 0.9813)$$

Table 3.4 Dipole polarisability (α)

Target	Available α (Å)^3	Present predicted α (Å)^3
HD	0.7910 [21]	-
D_2	0.7830 [21]	-
D_2O	1.4530 [21]	-
ND	-	1.3589
ND_2	1.8420 [21]	-
ND_3	2.1580 [21]	-
SiD	-	4.2157
SiD_2	-	4.1719
SiD_3	-	4.8701
CD_2	1.7750 [42]	-
CD_3	2.1700 [42]	-
CD_4	2.5230 [21]	-

These relationships allowed us to forecast the polarisability of ND, SiD, SiD_2, and SiD_3 molecules, which, to the best of our knowledge, is not available in the literature (Table 3.4).

3.2 H_2SO_4 (sulfuric acid)

Sulfuric acid (H_2SO_4) is produced from the oxidation of Sulphur dioxide (SO_2), the principal sulphur-containing substance mainly produced by humans, which is directly released into the atmosphere [43]. All the terrestrial planets once had liquid water, as shown by isotopic and geological evidence. Atmospheric H_2SO_4 is mostly the result of oxidation of sulphur dioxide by hydroxyl radical (OH) in the gas phase [44],

$SO_2 + OH \rightarrow HSO_3$

$HSO_3 + O_2 \rightarrow SO_3 + HO_2$

$SO_3 + 2H_2O \rightarrow H_2SO_4 + H_2O$

In addition, evidence from geological studies indicates that Mercury, Venus, Earth, and Mars all had periods of volcanic activity in their past. Sulphur dioxide, which is soluble in water, is also a common component of volcanic degassing and by undergoing the oxidation process, it generates the H_2SO_4 [45]. Moreover, Venus's atmosphere contains H_2O + H_2SO_4 solution clouds [45]. This H_2SO_4 is now known to have a crucial role in atmospheric nucleation [46,47].

Atmospheric nucleation and the continuous growth of newly produced particles are the main sources of atmospheric aerosol particles. These aerosol particles influence Earth's climate [48]. The aerosol particles reduce the temperature by diffusing sunlight. Aerosols in the troposphere can also change the size of cloud particles, which in turn modifies the properties of clouds to reflect and to absorb the sunlight. This has an impact on the Earth's energy budget. Strikingly, these pollutants deplete the protective ozone layer well above the Earth's surface [49]. The secondary electrons produced by cosmic ray particles and solar radiation have an impact on the molecules in the atmosphere. Hence, the primary natural phenomenon in the atmosphere is the interaction of electrons with atmospheric molecules. Ionization processes are the most fundamental events that open up for impact energy above the ionisation threshold of the molecules. Thus, Q_{ion} of electron interactions with the molecules present in the atmosphere, are crucial in astro-sciences, radio sciences, plasma sciences, biological research, etc. [50].

Given its significance in the atmospheres of all the planets including Earth, H_2SO_4 was selected as the study's target system in this instance. The decision to conduct this work was prompted by the dearth of theoretical and experimental research on this chemical.

3.2.1 Theoretical Methodology

In the present work, the data of Q_{ion} for electron collision with H_2SO_4 has been reported for the energy from the molecular ionisation threshold to 5 keV. For this calculation, we have used CSP-ic (Complex Scattering Potential-ionization contribution) method. Since this is the first attempt to study the electron interactions with H_2SO_4, we have computed the Q_{ion} using various models. These models include Independent Atom Model (IAM) using atomic as well as molecular properties. Moreover, we have carried a study to understand the dependence of

Q_{ion} on the molecular IE and the molecular size through number of target electrons (Z) by evaluating Q_{ion} for H_3PO_4 which is having same number of electrons (Z = 50) as H_2SO_4 and comparing with cross sections of H_2SO_4. In Table 3.5 we show ionisation potential of the target atom/molecules [21a].

The data for the ionisation cross-sections, Q_{ion} for electron collisions with H_2SO_4 have been presented in the current work for energy range, target ionisation threshold to 5 keV [21b]. Q_{ion} calculation has been carried out by using a variety of models as this is the first attempt to analyse the electron interactions with H_2SO_4. Among these, is the Independent Atom Model (IAM) using both atomic and molecular attributes. In addition, we evaluated Q_{ion} for H_3PO_4, which has the same number of electrons (Z = 50) as H_2SO_4 and compared it to the Q_{ion} of H_2SO_4 in order to understand the influence of the molecular ionisation energies (IE) and the molecule size on the Q_{ion}. Ionisation potential of the target atoms or molecules is displayed in Table 3.5 [21].

Table 3.5 Ionisation Energies (IE) [21]

Target	IE (eV)	Target	IE (eV)	Target	IE (eV)
Hydrogen (H)	13.60	Sulphur (S)	10.36	Oxygen (O)	13.62
Phosphorus (P)	10.48	H_2SO_4	12.40	H_3PO_4	11.72

3.2.2 Results and Discussion

The total ionisation cross-sections (Q_{ion}) as well as Q_{inel} and Q_{exc}, for the gaseous H_2SO_4 on impact with electrons for energy ranging from close to the ionisation threshold to 5000 eV, have been given in the current section. There are no earlier findings available on H_2SO_4 to compare the present data. As a result, we used a variety of models to investigate the e^- - H_2SO_4 collision, and the outcomes are displayed in Figure 3.17. The Q_{ion} of H_2SO_4 is estimated using various approximations, including the Independent Atom model (IAM) with atomic and molecular ionisation energies (IE) for the constituent atoms. The cross-sections for IAM with atomic IEs and with molecular IEs are near to one another in Figure 3.18, which is an intriguing observation. One of the causes could be that, with the exception of

sulphur (S), the IEs of the constituent atoms H (IE = 13.60 eV), S (IE = 10.36 eV), O (IE = 13.62 eV), and H_2SO_4 (IE = 12.40 eV) are quite similar. The IE of oxygen (O) and hydrogen (H) in particular have values that are similar to the IE of H_2SO_4. Sulphur's IE is lower than the H_2SO_4's IE. Oxygen contributes much more than the sulphur when the cross-sections of the constituent atoms are included.

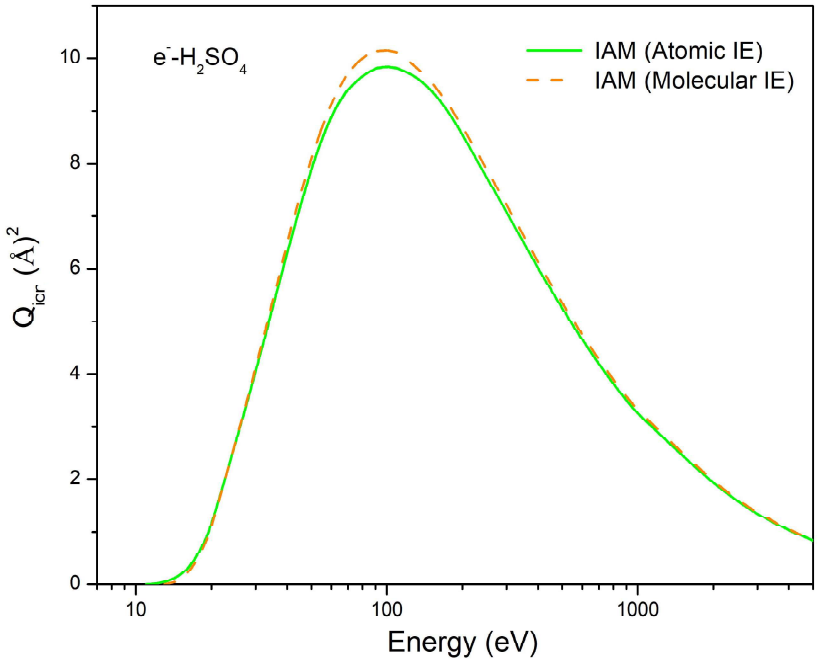

Figure 3.17 Present Q_{ion} for e^--H_2SO_4 collision

Red line: IAM with atomic IE, Green line: IAM with molecular IE

Figure 3.18 displays the e^- - H_2SO_4 results for Q_{inel}, Q_{ion}, and Q_{exc}. We have compared our target system with phosphoric acid (H_3PO_4), a different molecule with the same number of electrons as H_2SO_4 (Z = 50). As can be seen in figure 3.18, we have plotted the Q_{ion} for the molecules H_2SO_4 and H_3PO_4. The ionisation energy of the target system is particularly sensitive to the Q_{ion}. As can be observed, the results we calculated and those of Mozejko and Sanche for H_3PO_4 [51], show good agreement with one another. The cross sections of both the molecules appear to travel along the same route. One of the causes is that they have nearly similar IEs (11.72 eV for H_3PO_4 and 12.40 eV for H_2SO_4) and the same number of molecular electrons (i.e., Z = 50).

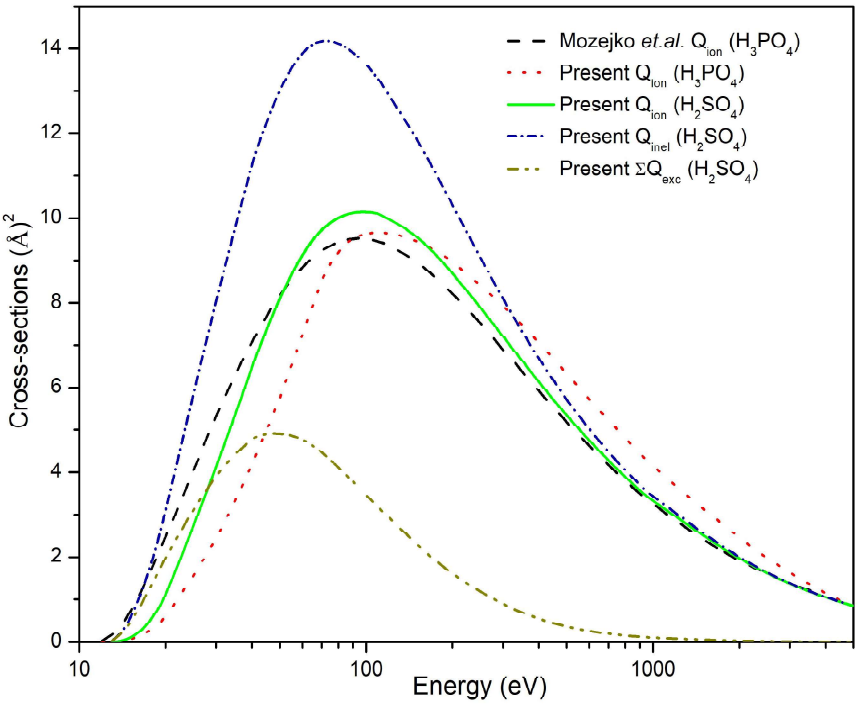

Figure 3.18 Cross-sections of H_2SO_4 and H_3PO_4

Solid: Present Q_{ion} of H_2SO_4; dash: Mozejko et.al. Q_{ion} for H_3PO_4 [51]*; dot: present Q_{ion} of H_3PO_4; short dash dot: present Q_{inel} of H_2SO_4 and dash dot dot: present Q_{exc} of H_2SO_4*

As a result, we can see that our Q_{ion} depends not only on the ionisation potential of the target molecule, but also on its size, or the number of electrons, because the molecular charge cloud acts as a scatterer.

3.3 Bibliography

[1] J. Liu and X. Liu, *Application of Deuterated Compounds*, in *Deuteride Materials* (Springer, Singapore, 2019), pp. 231–285.

[2] W. Y. Baek and B. Grosswendt, *Total Electron Scattering Cross Sections of He, Ne and Ar, in the Energy Range 4 EV 2 KeV*, Journal of Physics B: Atomic, Molecular and Optical Physics **36**, 731 (2003).

[3] T. D. Younger, S. M.; and Mark, *Semi-Empirical and Semi-Classical Approximations for Electron Ionization*, in *Electron Impact Ionization*, edited by G. H. Mark, T.D.; and Dunn (Springer, Vienna, Veinna, 1985), pp. 24–41.

[4] F. W. Taylor, S. K. Atreya, T. H. Encrenaz, D. M. Hunten, P. G. Irwin, and T. C. Owen, in *Jupiter: The Planet, Satellites and Magnetosphere*, edited by F. et. al. Bagenal (Cambridge University Press, Cambridge, 2004), pp. 59–78.

[5] N. J. Mason, J. M. Gingell, N. C. Jones, and L. Kaminski, *No Title*, Philosophical Transactions of the Royal Society of London. Series A: Mathematical, Physical and Engineering Sciences **357**, 1175 (1999).

[6] Donald Rapp, and P. Englander-Golden, *Total Cross Sections for Lonization and Attachment in Gases by Electron Impact. I. Positive Ionization*, J Chem Phys **43**, 1464 (1965).

[7] I. R. Cowling and J. Fletcher, Electron-Molecule Collision Ionization in Hydrogen and Deuterium, 1973.

[8] B. L. Schram, F. J. De Heer, M. J. Van Der Wiel, and J. Kistemaker, *IONIZATION CROSS SECTIONS FOR ELECTRONS (0.6-20 KeV) IN NOBLE AND DIATOMIC GASES*, Physica **31**, 94 (1965).

[9] T. D. Mark, and F. Egger, *CROSS-SECTfON FOR SINGLE ION-IZATION OF Hz0 AND DLO BY ELECTRON IMPACT FROM THRESHOLD UP TO 17OeV*, Inkrnarional Journal of Mass Specfronutry and Ion Physics **20**, 89 (1976).

[10] A. V. Snegursky, and A. N. Zavilopulo, *Electron Impact Ionization of D2O Molecules: Single Ionization Cross Section*, Scientific Herald of Uzhhorod University. Series Physics **6**, 207 (2000).

[11] V. Tarnovsky, H. Deutsch, and K. Becker, *Electron Impact Ionization of the Hydroxyl Radical*, Journal of Chemical Physics **109**, 932 (1998).

[12] H. C. Straub, B. G. Lindsay, K. A. Smith, and R. F. Stebbings, *Absolute Partial Cross Sections for Electron-Impact Ionization of H2O and D2O from Threshold to 1000 EV*, Journal of Chemical Physics **108**, 109 (1998).

[13] N. Lj. Djuric, I. M. Cadez, and M. V. Kurepa, *H2O AND D2O TOTAL IONIZATION CROSS-SECIIONS BY ELECTRON IMPACT*, Int J Mass Spectrom Ion Process **83**, R7 (1988).

[14] V. Tarnovsky, H. Deutsch, and K. Becker, Cross-Sections for the Electron Impact Ionization of NDx (x = 1-3), 1997.

[15] R. Rejoub, B. G. Lindsay, and R. F. Stebbings, *Electron-Impact Ionization of NH3 and ND3*, Journal of Chemical Physics **115**, 5053 (2001).

[16] V. Tarnovsky, H. Deutsch, and K. Becker, *Electron Impact Ionization of the SiDx (X=1-3) Free Radicals*, Journal of Chemical Physics **105**, 6315 (1996).

[17] B. L. Schram, M. J. Van Der Wiel, F. J. De Heer, and H. R. Moustafa, *Absolute Gross Ionization Cross Sections for Electrons (0.6-12 KeV) in Hydrocarbons*, J Chem Phys **44**, 49 (1966).

[18] V. Tarnovsky, A. Levin, H. Deutsch, and K. Becker, Electron Impact Ionization of (x = 1-4) Electron Impact Ionization of CD x (x = 1-4), 1996.

[19] F. A. Baiocchi, R. C. Wetzel, and R. S. Freund, *Electron-Impact Ionization and Dissociative Ionization of the CD 3 and CD 2 Free Radicals*, Phys Rev Lett **53**, 771 (1984).

[20] H. L. Cox and R. A. Bonham, *Elastic Electron Scattering Amplitudes for Neutral Atoms Calculated Using the Partial Wave Method at 10, 40, 70, and 100 KV for Z = 1 to Z = 54*, J Chem Phys **47**, 2599 (1967).

[21] a) D. R. Lide, *CRC Handbook of Chemistry and Physics* (CRC Press, Boca Raton FL 2005, n.d.).

b) Smruti Parikh, Chetan Limbachiya, K. N. Joshipura, *Calculations of Total Ionization Cross-Sections for Electron Impact on H_2SO_4*, In: V. Singh, R. Sharma, M. Mohan, M. S. Mehata, A. K. Razdan, (eds) Proceedings of the International Conference on Atomic,

Molecular, Optical & Nano Physics with Applications. Springer Proceedings in Physics, vol **271**. Springer, Singapore (2020)

[22] S. Cotton, *Heavy Water Deuterium Oxide, D2O*, https://doi.org/10.6084/m9.figshare.5255143.v1.

[23] a) Mattia Melosso, Luca Bizzocchi, Filippo Tamassia, Claudio Degli Esposti, Elisabetta Cane, and L. Dore, *The Rotational Spectrum of 15ND. Isotopic-Independent Dunham-Type Analysis of the Imidogen Radical*, Physical Chemistry Chemical Physics **21**, 3564 (2019).

b) Smruti Parikh, Minaxi Vinodkumar, and Chetan Limbachiya, *Electron impact inelastic molecular processes for deuterated compounds*, Chemical Physics **565**, 111766 (2023).

[24] A. Pospieszczyk, S. Brezinsek, G. Sergienko, P. T. Greenland, A. Huber, A. Meigs, Ph. Mertens, U. Samm, M. Stamp, and S. Wiesen, *No Title*, Journal of Nuclear Materials **337–339**, 500 (2005).

[25] E. M. Hollmann, S. Brezinsek, N. H. Brooks, M. Groth, A. G. McLean, A. Y. Pigarov, and D. L. Rudakov, *Spectroscopic Measurement of Atomic and Molecular Deuterium Fluxes in the DIII-D Plasma Edge*, Plasma Phys Control Fusion **48**, 1165 (2006).

[26] S. Brezinsek, P. T. Greenland, Ph. Mertens, A. Pospieszczyk, U. Samm, B. Schweer, and G. Sergienko, *Formation of HD Molecules in the Boundary Layer of TEXTOR*, Phys Scr **T103**, 63 (2003).

[27] J. S. Yoon, Y. W. Kim, D. C. Kwon, M. Y. Song, W. S. Chang, C. G. Kim, V. Kumar, and B. J. Lee, *Electron-Impact Cross Sections for Deuterated Hydrogen and Deuterium Molecules*, Reports on Progress in Physics **73**, (2010).

[28] H. M. Butner, S. B. Charnley, C. Ceccarelli, S. D. Rodgers, J. R. Pardo, B. Parise, J. Cernicharo, and G. R. Davis, *Discovery of Interstellar Heavy Water*, Astrophys J **659**, L137 (2007).

[29] N. Djuric´, D. Djuric´, S. Zhou, G. H. Dunn, and M. E. Bannister, Electron-Impact Dissociative Excitation of CD n "n25…: Detection of Light Fragment Ions, 1998.

[30] D. C. Lis, E. Roueff, M. Gerin, T. G. Phillips, L. H. Coudert, F. F. S. van der Tak, and P. Schilke, *Detection of Triply Deuterated Ammonia in the Barnard 1 Cloud*, Astrophys J **571**, L55 (2002).

[31] F. F. S. van der Tak, P. Schilke, H. S. P. Müller, D. C. Lis, T. G. Phillips, M. Gerin, and E. Roueff, *Triply Deuterated Ammonia in NGC 1333*, Astron Astrophys **388**, L53 (2002).

[32] A. Bacmann et al., *First Detection of ND in the Solar-Mass Protostar IRAS16293-2422*, Astron Astrophys **521**, L42 (2010).

[33] A. Bacmann, F. Daniel, P. Caselli, C. Ceccarelli, D. Lis, C. Vastel, F. Dumouchel, F. Lique, and E. Caux, *Stratified NH and ND Emission in the Prestellar Core 16293E in L1689N*, Astron Astrophys **587**, A26 (2016).

[34] T. G. Ference, J. S. Burnham, W. F. Clark, T. B. Hook, S. W. Mittl, K. M. Watson,and Liang-Kai Kevin Han, *He Combined Effects of Deuterium Anneals and Deuterated Barrier-Nitride Processing on Hot-Electron Degradation in MOSFET's*, IEEE Trans Electron Devices **46**, (1999).

[35] William F. Clark, Thomas G. Ference, Terence B. Hook, Dale W. Martin, *Use of Deuterated Materials in Semiconductor Processing*, US 5,972,765 (1999).

[36] Richard W. Gregor, Isik C. Kizilyalli, *Deuterated Direlectric and Polysilicon Film-Based Semiconductor Devices and Method of Manufacture Thereof*, 6,023,093 (n.d.).

[37] Joseph W. Lyding, Karl Hess, *Forming of Deuterium Containing Nitride Spacers and Fabrication of Semiconductor Devices*, 6,147,014 (2000).

[38] E. M. Breitung, *Optical Waveguide Devices with Deuterated Amorphos Carbon Core Structures*, US 7,006,753 B2 (2006).

[39] J. Lecointre, D. S. Belic, J. J. Jureta, R. Janev, and P. Defrance, *Absolute Cross Sections and Kinetic Energy Release Distributions for Electron-Impact Ionization and Dissociation of CD+4*, The European Physical Journal D **50**, 265 (2008).

[40] J. Lecointre, S. Cherkani-Hassani, D. S. Belic, J. J. Jureta, K. Becker, H. Deutsch, T. D. Märk, M. Probst, R. K. Janev, and P. Defrance, *Absolute Cross Sections and Kinetic Energy Release Distributions for Electron Impact Ionization and Dissociation of CD+*, Journal of Physics B: Atomic, Molecular and Optical Physics **40**, 2201 (2007).

[41] P. W. Harland and C. Vallance, *Ionization Cross-Sections and Ionization Efficiency Curves from Polarizability Volumes and Ionization Potentials*, Int J Mass Spectrom Ion Process **171**, 173 (1997).

[42] D. G. LeGrand and G. L. Gaines Jr., *The Polarizability of Some Deuterated Hydrocarbons*, Journal of Physical Chemistry **98**, 4842 (1994).

[43] D. Salcedo, P. W. Villalta, V. Varutbangkul, and J. C. Wormhoudt, *Appendix C : Effect of Relative Humidity on the Detection of Sulfur Dioxide and Sulfuric Acid Using a Chemical Ionization Mass Effect of Relative Humidity on the Detection of Sulfur Dioxide and Sulfuric Acid Using a Chemical Ionization Mass Spectrometer*, Int J Mass Spectrom **231**, 17 (2004).

[44] John T. Jayne, Ulrich Poschl, Yu-min Chen, David Dai, Luisa T. Molina, Douglas R. Worsnop, Charles E. Kolb, and M. J. Molina, *Pressure and Temperature Dependence of the Gas-Phase Reaction of SO3 with H2O and the Heterogeneous Reaction of SO3 with H2O/H2SO4 Surfaces*, Journal of Physical Chemistry A **101**, 10000 (1997).

[45] K. Mcgouldrick, O. B. Toon, and D. H. Grinspoon, *Sulfuric Acid Aerosols in the Atmospheres of the Terrestrial Planets*, Planet Space Sci **59**, 934 (2011).

[46] L. Yao, O. Garmash, F. Bianchi, J. Zheng, C. Yan, P. Paasonen, M. Sipilä, M. Wang, X. Wang, and S. Xiao, Atmospheric New Particle Formation from Sulfuric Acid and Amines in a Chinese Megacity, 2018.

[47] Mikko Sipila, Torsten Berndt, Tuukka Petaja, David Brus, Joonas Vanhanen, Frank Stratmann, Johnna Patokoski, Roy L. Mauldin III, Antti-Pekka Hyvarinen, Heikki Lihavainen, Markku Kulmala, *The Role of Sulfuric Acid in Atmospheric Nucleation*, Science **327**, 1243-1246 (2010).

[48] U. Lohmann, and J. Feichter, *Global Indirect Aerosol Effect-a Review*, Atmos Chem Phys **5**, 715 (2005).

[49] B. Allen, *Atmospheric Aerosols: What Are They, and Why Are They So Important?*, https://www.nasa.gov/centers/langley/news/factsheets/Aerosols.html.

[50] Mohit Swadia, Yogesh Thakar, Minaxi Vinodkumar, and Chetan Limbachiya, *Theoretical Electron Impact Total Cross Sections for Tetrahydrofuran (C4H8O)*, The European Physical Journal D **71**, 85 (2017).

[51] P. Mozejko, and L. Sanche, *Cross Sections for Electron Scattering from Selected Components of DNA and RNA*, Radiation Physics and Chemistry **73**, 77 (2005).